POLITECNICO DI TORINO
Repository ISTITUZIONALE

The effect of powder reuse on the surface chemical composition of the Scalmalloy powder in Powder Bed Fusion – Laser Beam process

(Article begins on next page)

28 April 2024

The effect of powder reuse on the surface chemical composition of the Scalmalloy powder in Powder Bed Fusion – Laser Beam process

A. Martucci[1], P.L. Tam[2], A. Aversa[1], M. Lombardi[1], L. Nyborg[2]

[1] Department of Applied Science and Technology, Politecnico di Torino, Torino, Italy.

[2] Department of Industrial and Materials Science, Chalmers University of Technology, Gothenburg, Sweden.

Abstract

The powder quality is one of the main factors to be considered in Laser Powder Bed Fusion (PBF-LB/M) production closely connected with the performance of the final component. Only powders with spherical particles, a low percentage of satellites, a narrow particle size distribution, controlled internal defects and a strongly limited surface oxide layer are acceptable for PBF-LB/M production. Gas atomisation is the main production method that permits to achieve the restrictive standards of the PBF-LB/M powder, however, it is energy-intensive and characterised by limited productivity. These considerations justify the key role of the reuse of the unmelted metal powder in obtaining a more sustainable PBF-LB/M process. Nevertheless, the reuse of the powder leads to significant changes in the particle morphology, particle size distribution and surface chemical composition, which can compromise the bulk properties. Powder surface oxide is one of the most impactful problems for the PBF-LB/M production, and Al-based alloys are particularly prone to this phenomenon. With the aim to study the effect of the powder reuse, a surface chemical analysis on gas atomised Scalmalloy powder was performed through the x-ray photoelectron spectroscopy investigation before and after seven jobs with thirty-two hours as overall build time. Results obtained for virgin and recycled Scalmalloy powders revealed remarkable differences in depth and composition of the surface oxide layer. The 57 % increase in the oxide layer thickness and the formation of carbides during PBF-LB/M production can have harmful effects on bulk properties.

Introduction

The metal Additive Manufacturing (AM) field has recorded significant growth in recent years thanks to the possibility of designing functional components with complex shapes [1]. Among the many AM techniques, the Laser Powder Bed Fusion (PBF-LB/M) stands out [2]. During this advanced process, the powder bed is molten by a focused laser beam in a layer-wise fashion, ensuring an efficient method to produce complex-shaped products with high performance [3]. The powder bed packaging and the powder spreadability play an essential role in the PBF-LB/M process.

PBF-LB/M powders must therefore have strict characteristics, among others, particle size distribution (PSD), morphology, related powder density (bulk and tap density) and flowability [4]. Balbaa et al. investigated the influence of virgin powder PSD on flow and packing properties, concluding that a higher mean size leads to better powder behaviour during the PBF-LB/M process [5]. In fact, fine powders proved to decrease the quality of powder layers and thus decrease the densification level achieved after bulk production [5-7]. Mussatto et al. focused their research on virgin powder morphology, studying how particle sphericity and surface texture impact the powder bed topography in spread layers [8]. In addition, simulating through the discrete element method, it turns out that

larger particle aspect ratios led to smaller packing density and higher surface roughness of spread layers [9]. PSD evaluations, as well as morphology and flowability, are specifically targeted for virgin characterisation to quickly identify the most suitable powders for PBF-LB/M production.

Among the different powder production methods, gas atomisation has proved to be the most suitable for the PBF-LB/M process, ensuring higher sphericity and packing density [10]. However, the gas atomisation process is expensive, energy-intensive, and characterised by limited productivity. In order to make the PBF-LB/M process sustainable and cost perspective, the powder is typically recycled. The understanding of the powder degradation after the PBF-LB/M process is however limited. In addition, no standardised procedure exists for the characterisation of recycled powders. Studies have demonstrated that the reuse of powders leads to significant changes in the particle morphology and particle size distribution, which can compromise the flowability, packing density of the powder bed and the laser-metal interaction [11, 12]. As reported by Cordova et al., in some cases, these changes in powder properties might result in higher porosity values in samples built with the recycled powder [13]. In addition to these complications, issues typical of some alloys that may be emphasised after the PBF-LB/M process must be considered.

Aluminium-based powders, among others, tend to oxidise and form Al_2O_3 and MgO layers on the surface [14]. Thermodynamic stability of the oxides and the thermal history of the metal surface determine the characteristics of the surface oxide [15]. In particular, the thickness, structure and composition of the formed oxide are influenced by the temperature and exposure time in combination with the potential oxidation of the surrounding atmosphere [16]. During the PBF-LB/M process the oxide content present in the feedstock material results in the formation of an oxide skin on the molten pool that creates a melt pool with an obtuse contact angle reducing the wettability [17]. The reduced wettability could result in un-melted particles during bulk production, as observed by Read et al. in AlSi10Mg samples [18]. In addition, the inhibition of the local consolidation could lead to the creation of crack nucleation sites, drastically reducing the fatigue life of the final component [19].

The present work aims to expand the knowledge on the Scalmalloy reuse effects on the surface oxide layer formation. Scalmalloy is a high-performance Al-based alloy, developed and patented by APWORKS [20]. This alloy achieved improved elongation, good corrosion resistance and weldability compared to the traditional Al alloys [21]. An extensive work on the importance of powder characterisation of this promising alloy was performed by Spierings et al. [22]. However, to the best of the authors' knowledge, only limited attention has been paid to the effect of Scalmalloy powder reuse. Although Cordova et al. focused their study on the reuse effects on powder morphology, particle size distribution and thus the bulk properties [13], an in-depth study of how the surface composition of Scalmalloy powders changes after several hours of PBF-LB/M production remains to be carried out.

For this reason, a surface chemical analysis was performed through the x-ray photoelectron spectroscopy (XPS) investigation on gas atomised Scalmalloy powder in the as-received state and after seven jobs with 32 hours as overall build time. In particular, a compositional analysis of the entire spectrum and a detailed investigation of the chemical states of specific elements were conducted. The results revealed significant differences in depth and composition of the surface oxide layer of the virgin and recycled Scalmalloy powders that could lead to a potentially harmful effect on bulk properties.

Materials and methods

A gas atomised Scalmalloy powder supplied by Höganäs AB, Sweden was selected for the present study. The chemical composition calculated by Höganäs AB using the inductively coupled plasma (ICP-AES) was reported in Table 1.

Table 1: Scalmalloy powder chemical composition in as-received condition

Condition (in wt%)	Mg	Sc	Zr	Mn	Fe	Si	Al
As atomised	4.7	0.7	0.27	0.48	0.12	0.06	Remainder

The powder was analysed in virgin condition (as atomised) and in a recycled state after seven PBF-LB/M jobs with an overall build time of 32 hours. Strict procedures were adopted during the powder processing and storage to avoid any cause of contamination or oxidation. In particular, all PBF-LB/M jobs were performed under the same conditions: an inert atmosphere (Argon) with an O_2 level <0.1% (<1000 ppm) was used for the entire process; no platform heating was applied; process parameters and job geometry were always the same. The unmelted powder was sieved below 50 μm after each job, and no fraction of virgin powder was added between jobs. In addition, all the powder samples were stored in a humidity- and temperature-controlled environment. In order to conduct an accurate systematic study, particular attention was placed on the sampling procedure. Before conducting the XPS analysis, the powder was sprinkled on the surface of the sticky carbon conductive tape for both the virgin and the used sample. A PHI 5000 VersaProbe III Scanning XPS Microprobe™ (ULVAC-PHI Inc.) was used to perform the chemical analysis. X-rays were generated by a monochromatic Al Kα source (1486.6 eV). To prevent possible contamination during etching, the XPS analysis was conducted under an ultra-high vacuum (UHV) condition at a level below 5 x 10^{-8} Pa, and only one sample was introduced in the chamber each time. Considering the mentioned conditions, the reoxidation rate should be very slow, and the chance of inter-contamination could be regarded as impossible. Argon is the only element that comes from the sputtering medium of the ion gun, that is, in the form of argon ions (Ar^+). For this reason, the only and unavoidable contamination can only come from argon. The binding energy scale in the system was aligned with the core level peaks of sputtered gold ($Au4f_{7/2}$ = 83.96 eV), silver ($Ag3d_{5/2}$ = 368.23 eV) and copper ($Cu2p_{3/2}$ = 932.64 eV) according to ISO 15472 standard. Two scan modes were conducted: a wide energy range survey scan to evaluate the surface composition and a narrow scan in a selected energy region to analyse the chemical state of individual elements of interest. In XPS, the photoelectron peaks are denoted according to the spectroscopic notation of the core levels they come from (1s, 2s, 2p, etc). Selected region spectra were recorded covering the C1s, O1s, Mg2p, Al2p, Sc2p and Zr3d peaks. The obtained photoelectron peaks were curve fitted using the PHI Multipak software (ULVAC-PHI). In particular, a Shirley background and a Gauss-Lorentzian function were used for peak fitting. Depth compositional profiling was done by alternating argon ion etching and XPS measurement. The survey measurement on each sample, i.e. virgin and reused powders, were repeated twice and showed good repeatability prior to depth profiling experiments.

Results

The survey spectra of Scalmalloy virgin and the recycled powders display the presence of C, O, Mg, Al, Sc and Zr peaks on the surface (Fig. 1).
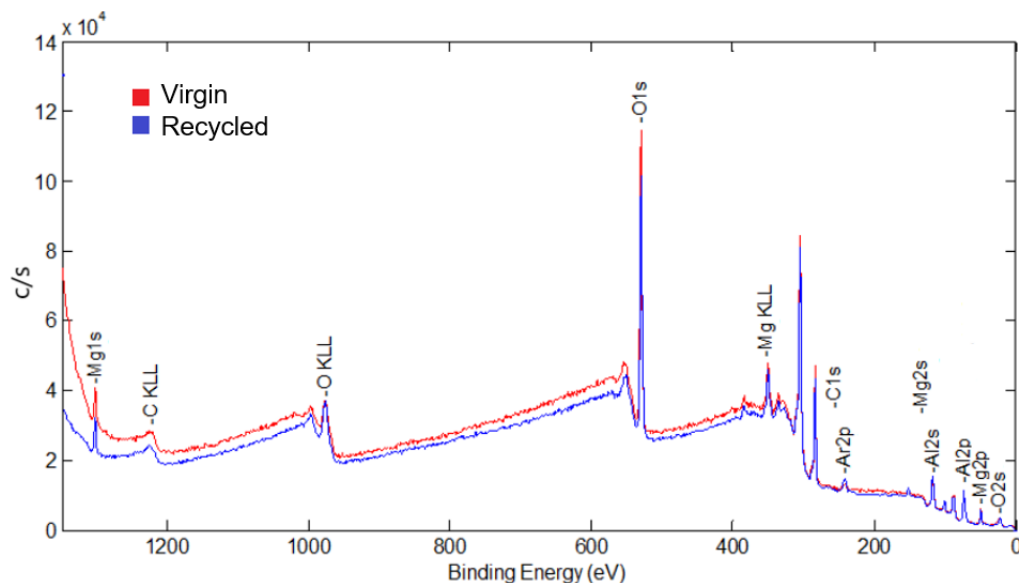
Figure 1: XPS survey scan of Scalmalloy virgin and recycled powders at 0 Å.

The survey scan on each sample did repeat twice with good repeatability, as easily visible in Table 2.

Condition (in at.%)	C	O	Mg	Al	Si	Ar	Sc	Zr
Virgin	32.8	46.0	6.7	11.9	2.0	0.5	0.17	0.0
(Standard deviation)	0.9	1.3	0.3	0.6	0.3	0.1	0.25	0.0
Recycled	26.9	52.6	7.8	11.4	1.2	0.8	0.14	0.0
(Standard deviation)	2.0	0.2	0.6	0.9	0.3	0.1	0.20	0.0

Table 2: Chemical compositions obtained through the survey scan of Scalmalloy virgin and recycled powders at Å.

The small standard deviations from the survey scan, reported in Table 2, suggest high measurement accuracy, with the exception of two elements, Sc and Zr. Respecting the standardised composition of Scalmalloy, Sc and Zr are present in the alloy in small amounts (0.7 and 0.27 wt%, respectively) and consequently do not allow for acceptable spectral quality. Based on these considerations and the unreliable values recorded, it was decided to exclude further investigations of Sc and Zr from the present study. Plotting the compositional depth profiles (with reference to Al_2O_3 calibration), it is observed that the O content decreases along the sputtered depth (Fig. 2). This decremental trend is sharper in the virgin powder profile. Furthermore, the oxygen content never reaches zero percent even at the innermost depth of this investigation. In both conditions, the carbon level drops immediately after the earliest layers and remains almost constant after 900 Å. The major metallic ingredients in the powder are Al and Mg in both samples. The aluminium content starts at values close to 10 at.% for both conditions and then increases to the standard values for the Scalmalloy composition. On the other hand, the presence of magnesium appears to be more marked for the upper layers of the powder and then decreases. In particular, the Mg level drops from around 10 to 0.5 at.% along the depth profile for virgin powder and to 2 at.% for the processed one.
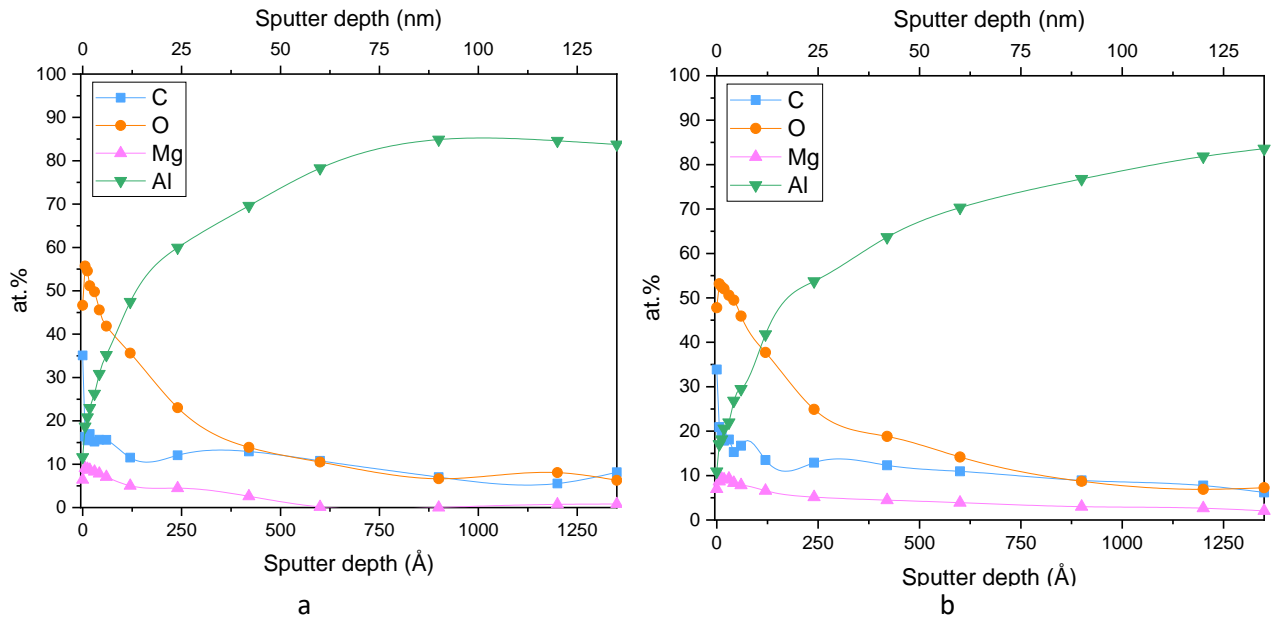
Figure 2: Compositional depth profiles with reference to Al₂O₃ calibration in virgin (a) and recycled (b) conditions.

Through the narrow scans analysis, it was possible to understand the chemical state distribution of the main element along the sputter depth (always with reference to Al_2O_3 calibration). As shown in Fig. 3a and Fig. 3b, aluminium appears in a binary state: metallic (72.8 eV) and oxidised (75.4 eV). As highlighted by the red trend, the dominant state in the outermost layers is the oxidised state for both powders conditions. Observing the narrow scans regarding the virgin powder in Fig. 3a, the Al in oxide state remains predominant until 30 Å (reported in blue) and a trend reversal occurs at 42 Å (reported in green). As reported in Fig. 3b, the transition from the predominance of the oxide state to the metallic state occurs at 60 Å (green line) for the recycled powder. Fitting the narrow scan curves with the PHI Multipak software, it was possible to extrapolate the areas under the peaks and thus obtain the chemical state distribution along sputter depth for the virgin powder (Fig. 3b) and the recycled one (Fig. 3c). These graphs confirm the trend reversal explained above and reveal that Al_2O_3 remains observable even in the innermost analysed layers. In particular, at 1350 Å the area under the Al_2O_3 peak is 15 % for the as-received powder and 25 % for the processed one. These values correspond to an amount of Al_2O_3 of 4.2 and 6 at.%, for virgin and recycled powder respectively.
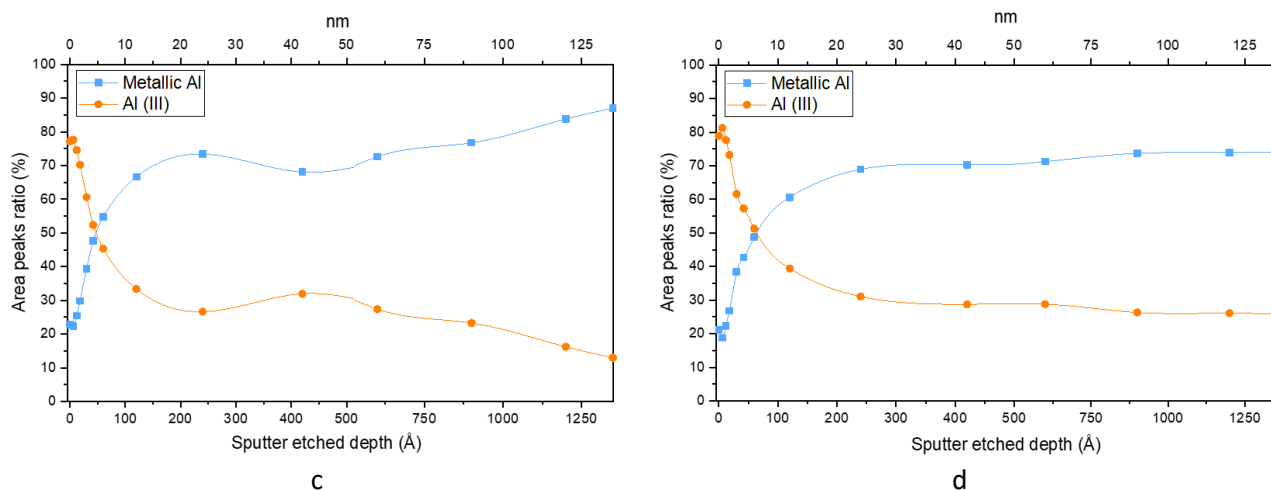
c

d
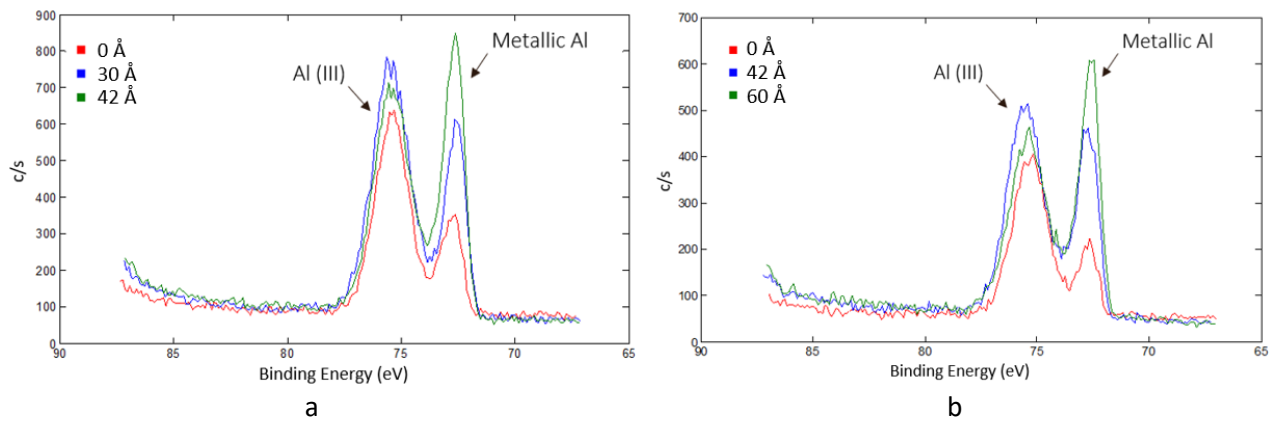
Figure 3: Al narrow scans and related chemical state distribution along sputter depth (with reference to Al_2O_3 calibration) in virgin (a,c) and recycled (b,d) conditions.

The binary chemical states (metallic and oxidised) are also visible in the Mg chemical state distribution displayed in Fig. 4. However, the lower content of Mg with respect to Al implies a noisier background that makes peak visualisation more difficult (Fig. 4a and Fig. 4b). Relying on the chemical state distribution along sputter depth obtained after curves fitting, the inversion from the oxidised to the metallic state occurs at 600 Å for the virgin powder and 900 Å for the processed one (Fig. 4c and Fig. 4d).
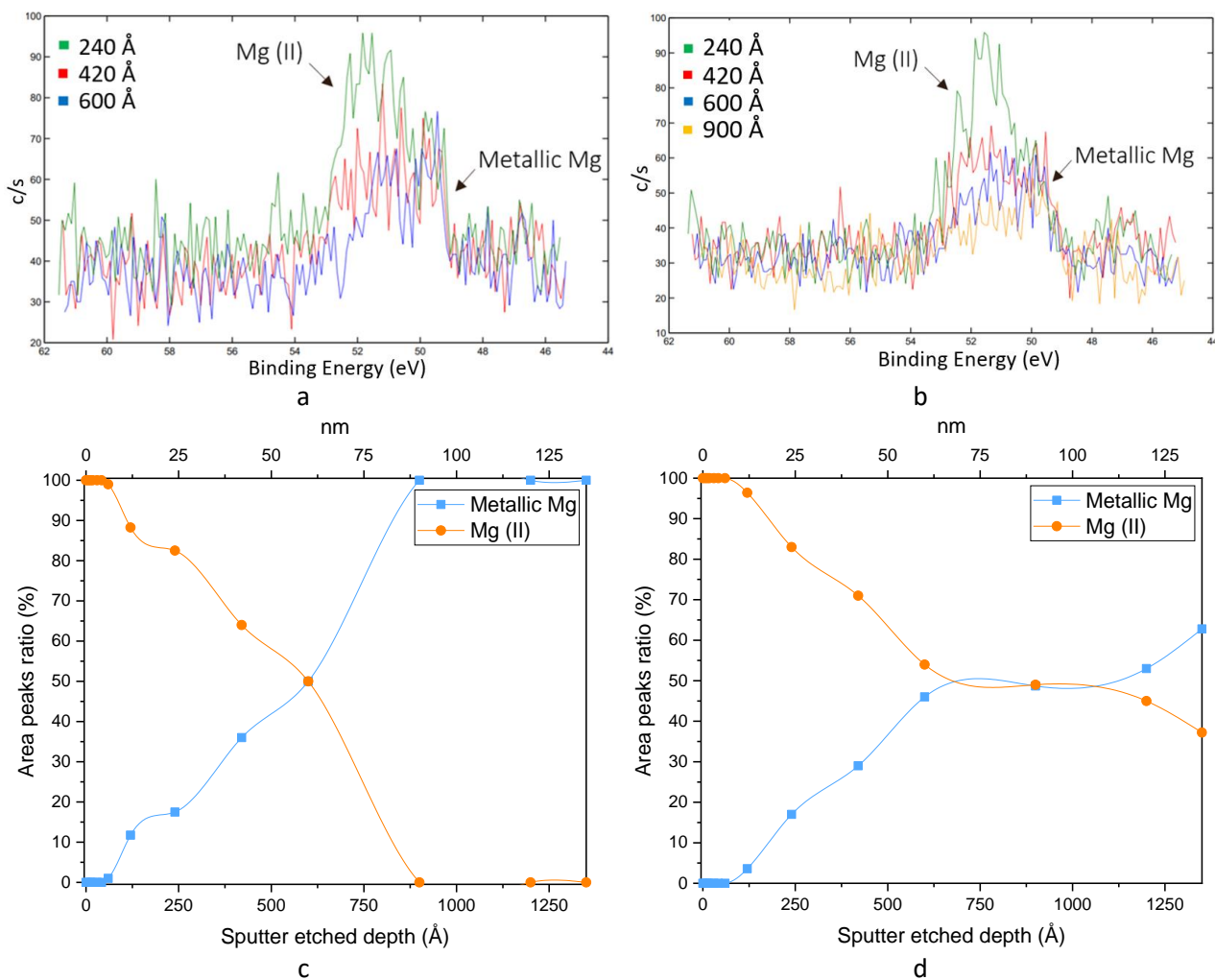

a

b

c

d

Figure 4: Mg narrow scans and related chemical state distribution along sputter depth (with reference to Al_2O_3 calibration) in virgin (a,c) and recycled (b,d) conditions.

Starting from the Al(III) and Mg(II) trend in Fig. 3 and Fig. 4 and transforming these quantities in at.%, an atomic ratio of 2:1 for Al_2O_3 and MgO can be calculated for the first 1.8 nm. Then, the Al_2O_3 prevails more overwhelmingly.

The main carbon peak on both powders is around 286.0 eV and it is related to adventitious carbon (i.e. surface contaminant). Both samples recorded a small carbonate-related peak at the uppermost layers (below 18 Å). From 900 Å, in the recycled powders scan, the peak positions of C1s move from 286 to 283.0 eV, revealing the change of form from adventitious carbon to carbide. Meanwhile, no carbide was detected in the virgin powder, even at the innermost measured depth.
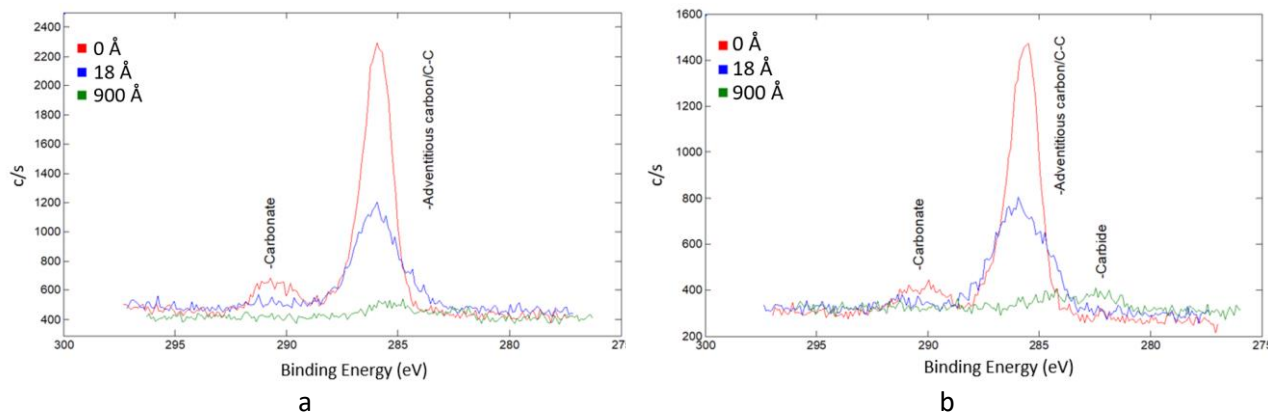

Figure 5: Chemical state of C at different sputter depth (with reference to Al_2O_3 calibration) in virgin (a) and recycled (b) conditions.

The oxide layer mainly consists of Al and Mg oxide (Al_2O_3 and MgO), their trends as a function of the analysed depth are expressed in at.% with an orange line in Fig. 6. The residual part goes to compose the hydroxides and other minor oxides which, together with the carbides, form the "other compounds" indicated in green. The elements in a metallic form that constitute the proper alloy are noted in purple. At the innermost analysed layer, the oxide mixture is still present at 4.2 at.% for the virgin sample and 7.3 at.% for the recycled one. Moreover, the alloy mixture became predominant over the oxide mixture after 18 and 42 nm for the as-received and processed powders, respectively.
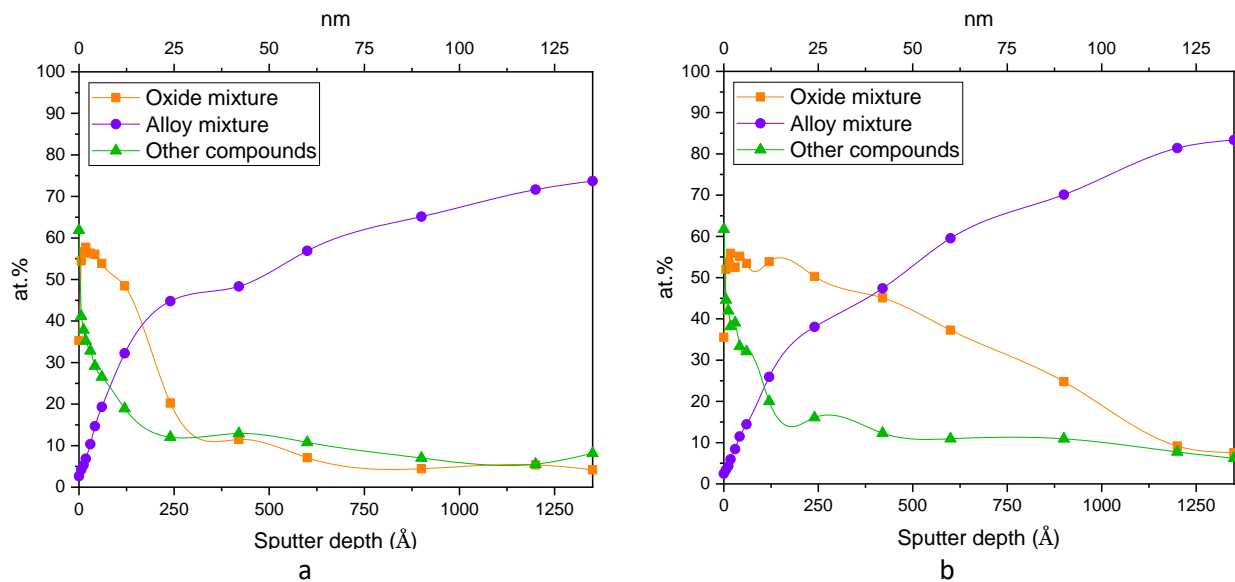
Figure 6: Overall chemical analysis in virgin (a) and recycled (b) powders as a function of the sputter depth (with reference to Al_2O_3 calibration).

Discussion

In order to make the PBF-LB/M process energy and economically sustainable, the recycling of powders becomes necessary. A strong relationship between powder recycling and the quality of the final part has been reported in the literature [22, 23]. As extensively demonstrated by Wang et al., the effects of reuse are highly dependent on the type of alloy [24]. In particular, aluminium is a strongly electronegative metal and its strong oxygen affinity explains the importance of monitoring the use of Al-based alloys in the PBF-LB/M process [25]. In addition to the oxides already present in the feedstock material, the residual oxygen in the PBF-LB/M build chamber exacerbates the oxidation issue [26]. In this study, the effect of PBF-LB/M powder reuse on the surface chemical composition of the Scalmalloy powder was in-depth studied through an XPS analysis. The ability to explore the first atomic layers and assign chemical states to detected atoms results in considering the XPS a powerful tool for the investigation of surface oxides in powders [27]. The oxidation tendency of this outstanding Al-based composition was confirmed in both powders conditions by the prominent O1s peak recorded in the survey scans (Fig. 1). Fig. 2 demonstrated that the presence of the oxide does not stop at the first layers of the powders. In fact, a residual presence of oxygen is still visible at the innermost analysed depth (135 nm) and is around 4.2 at.% for the virgin sample and 7.3 at.% for the recycled one. Considering the level whereby the oxygen content halves from the starting value, the oxidised layer is about 42 nm for the virgin powder and 60 nm for the processed powder (Fig. 2). The compositional depth profiles reported in Fig. 3 and Fig. 4 illustrated that oxides are predominantly based on Al and Mg. This deduction accords with Raza et al. and Trunov et al. observations, which stated that typical powder surface oxides in Al-based compositions with Mg are Al_2O_3 and MgO [28, 29]. Calculations from the survey scans suggest that for the first 1.8 nm, Al_2O_3 and MgO are in a 2:1 ratio for both samples. After that, the Al_2O_3 prevails more overwhelmingly. Looking closer at the chemical state distribution along sputter depth extracted from narrow scans, more accurate considerations of oxide composition can be obtained. From Fig. 3, it is easy to see that on the surface, aluminium is mainly in oxide form (75.4 eV). Continuing with ion etching, Al state changes to a predominantly metallic form around 4.2 and 6 nm, respectively for the virgin and recycled samples. However, the Al_2O_3 layer is much deeper, at 135 nm its presence is still visible at 4.2 at.% for the as-received powder and 6 at.% for the processed one. On the other hand, Mg on the surface is present exclusively in the oxidised state. The transition from oxidised to metallic dominance occurs at 60 nm for the virgin powder and 90 nm for the recycled powder. Moreover, if the MgO peak disappears to the XPS pattern after 90 nm in the virgin state, a residual presence of MgO is still visible in the innermost analysed layer of the recycled powder. These considerations imply that Mg is mostly diffused on the surface getting oxidised and that the depth of the MgO layer increases after the PBF-LB/M process. The higher atomic percentage of Al_2O_3 and MgO in the deeper layers of the recycled powder suggests that, after 32 hours of PBF-LB/M processing, a significant thickening of the oxide layer occurred. By combining the identified amounts of Al_2O_3 and MgO in the chemical state distribution, a unique trend was drawn and reported in Fig. 6. From the orange line of Fig. 6, it is evident that the oxide layer remains predominant up to 21 nm for the virgin powder and 33 nm for the recycled powder, with an increase of 57 % post PBF-LB/M process. Analysing the C peaks of Fig. 5 in the narrow scans it is possible to deduce that the presence of carbides is detectable only in the recycled powder down to 90 nm. Future investigations into the composition of the detected carbides

and possible causes of formation should be performed. However, it is important to emphasise that these are not homogenous layers of oxides over the entire powder surface but rather a patch structure whose depths are as reported in this paper. All of the above considerations lead to the definition of the importance to analyse powders after PBF-LB/M processing. After only 32 hours of processing, the 57 % increase in surface oxide thickness of the powders, as well as the carbide formation, is detected.

Conclusions

The present study sought to determine how the reuse of Scalmalloy powders after the PBF-LB/M process had an implication on the surface composition. The obtained results can be summarised as follows:

•   Both virgin and recycled Scalmalloy powders are covered by oxides and surface contaminant revealed as adventitious carbon;

•   Oxidation sensitive elements, such as Al and Mg, were found in high concentrations on the surface in both conditions. The O1s, Al2p and Mg2p spectra show that the main forms of oxides are Al_2O_3 and MgO;

• Al_2O_3 is the most abundant and its presence persists down to the innermost layers. A presence of 4.2 and 6 at.% respectively for the virgin and recycled samples is still visible at 135 nm;

•   Mg appears to be present mainly on the surface and in the oxidised state. In the XPS pattern related to the virgin powder the MgO peak disappears after 42 nm and then the Mg presence is exclusively in the metallic state. On the other hand, a residual 1.4 at.% of MgO is still detectable in the innermost investigated layer (135 nm) of the recycled powder;

•   After 32 hours of the PBF-LB/M process there was an increase in oxide thickness of around 57 % and the formation of carbides.

These results highlighted significant changes that occur to Scalmalloy powders after the PBF-LB/M process. Powder reuse is a turning point in achieving a sustainable PBF-LB/M production. However, the increase in the oxide layer thickness and the formation of carbides should have an adverse effect on the bulk properties. Examining the chemical state of the powder surfaces is, therefore, a necessary step. In addition, the present study paves the way for future quantitative analysis of the surface chemical states to understand the limiting conditions that do not affect the bulk properties. In particular, through XPS analysis, it could be possible to determine when powders reach a condition that is not compatible with a correct PBF-LB/M processing in order to save time and energy.

Acknowledgements

Bibliography

1. Blakey-Milner B, Gradl P, Snedden G, et al., Metal additive manufacturing in aerospace: A review. *Materials & Design*. 2021; 110008; ISSN 0264-1275
2. Kotadia HR, Gibbons G, Das A, Howes PD. A review of Laser Powder Bed Fusion Additive Manufacturing of aluminium alloys: Microstructure and properties. *Additive Manufacturing*. 2021; 46, 102155.
3. Yadroitsev I, Yadroitsava I, Du Plessis A. Basics of laser powder bed fusion. *Fundamentals of Laser Powder Bed Fusion of Metals*. Elsevier. 2021. 15-38.
4. Zegzulka J, Gelnar D, Jezerska L, et al. Characterization and flowability methods for metal powders. *Scientific Reports*. 2020; 10(1); 1-19.
5. Balbaa MA, Ghasemi A, Fereiduni E, et al. Role of powder particle size on laser powder bed fusion processability of AlSi10Mg alloy. *Additive Manufacturing*. 2021; 37; 101630.
6. Meier C, Weissbach R, Weinberg J, et al. Critical influences of particle size and adhesion on the powder layer uniformity in metal additive manufacturing. *Journal of Materials Processing Technology*, 2019; 266; 484-501.
7. Chen H, Wei Q, Wen S, Li Z, Shi Y. Flow behavior of powder particles in layering process of selective laser melting: Numerical modeling and experimental verification based on discrete element method. *International Journal of Machine Tools and Manufacture*. 2017; 123; 146-159.
8. Mussatto A, Groarke R, O'Neill A, Obeidi MA, Delaure Y, Brabazon D. Influences of powder morphology and spreading parameters on the powder bed topography uniformity in powder bed fusion metal additive manufacturing. *Additive Manufacturing*. 2021; 38; 101807.
9. Haeri S, Wang Y, Ghita O, Sun J. Discrete element simulation and experimental study of powder spreading process in additive manufacturing. *Powder Technology*.2017; 306; 45-54.
10. Li R, Shi Y, Wang Z, Wang L, Liu J, Jiang W. Densification behavior of gas and water atomized 316L stainless steel powder during selective laser melting. *Applied surface science*. 2010; 256(13); 4350-4356
11. Powell D, Rennie AE, Geekie L, Burns N. Understanding powder degradation in metal additive manufacturing to allow the upcycling of recycled powders. *Journal of Cleaner Production*. 2020; 268; 122077.
12. Santecchia E, Spigarelli S, Cabibbo M. Material reuse in laser powder bed fusion: side effects of the laser—metal powder interaction. *Metals*. 2020; 10.3; 341.
13. Cordova L, Bor T, de Smit M, Carmignato S, Campos M, Tinga T. Effects of powder reuse on the microstructure and mechanical behaviour of Al–Mg–Sc–Zr alloy processed by laser powder bed fusion (PBF-LB/M). *Additive manufacturing*. 2020. 36; 101625.
14. Raza A, Fiegl T, Hanif I, et al. Degradation of AlSi10Mg powder during laser based powder bed fusion processing. *Materials & Design*. 2021; 198; 109358.
15. Shvab R, Leicht A, Hryha E, Nyborg L. Characterization of the virgin and recycled nickel alloy HX powder used for selective laser melting. *European PM Conference Proceedings*. 2016; 1-6.
16. Hryha E, Shvab R, Gruber H, Leicht A, Nyborg L. Surface oxide state on metal powder and its changes during additive manufacturing: An overview. *Metall. Ital*. 2018; 3; 34-39.

17. Louvis E, Fox P, Sutcliffe CJ. Selective laser melting of aluminium components. *Journal of Materials Processing Technology*. 2011; 211(2); 275-284.

18. Read N, Wang W, Essa K, Attallah MM. Selective laser melting of AlSi10Mg alloy: Process optimisation and mechanical properties development. *Materials & Design*. 2015; 65; 417-424.

19. Moghimian P, Poirié T, Habibnejad-Korayem M, et al. Metal powders in additive manufacturing: A review on reusability and recyclability of common titanium, nickel and aluminum alloys. 2021; 43; 102017.

20. Sutcliffe C, Fox P. Manufacture of Metal Articles. WO2013179017A1, 5 December 2013.

21. Begoc S, Montredon F, Pommatau G, Leger G, Gas M, Eyrignoux S. Additive manufacturing of Scalmalloy® satellite parts. *In Proceedings of the 8th European Conference for Aeronautics and Space Sciences (EUCASS)*. 2019; 1-4.

22. Spierings, A. B. (2018) 'Powder Spreadability and Characterization of Sc- and Zr-modified Aluminium Alloys processed by Selective Laser Melting', BRISK Binary Robust Invariant Scalable Keypoints. Available at: https://doi.org/10.3929/ethz-a-010025751.

23. Weiss C, Munk J, Haefner CL. Investigation towards AlSi10Mg powder recycling behavior in the PBF-LB/M process and its influences on mechanical properties. 2021. *In 2021 International Solid Freeform Fabrication Symposium*. University of Texas at Austin.

24. Wang, Xuying, et al. "Bioaccessibility and reactivity of alloy powders used in powder bed fusion additive manufacturing." Materialia 19 (2021): 101196.

25. Sheasby PG, Pinner R, Wernick S. The surface treatment and finishing of aluminium and its alloys. *Materials Park, OH: ASM international*. 2001

26. Sun Z, Tan X, Tor SB, Sun Z, Tan X, Tor SB. Effects of chamber oxygen concentration on microstructure and mechanical properties of stainless steel 316L parts by selective laser melting. *In Proc. 3rd Int. Conf. Progess Addit. Manuf*. 2018; 470-475.

27. Wanger CD, Riggs WM, Davis LE, Moulder JF, Muilen GE. Handbook of X-ray Photoelectron Spectroscopy. *Perkin-Elmer Corporation*.1979.

28. Raza A, Fiegl T, Hanif I, et al. Degradation of AlSi10Mg powder during laser based powder bed fusion processing. *Materials & Design*. 2021; 198; 109358.

29. Trunov MA, Schoenitz M, Zhu X, Dreizin EL. Effect of polymorphic phase transformations in Al_2O_3 film on oxidation kinetics of aluminum powders. *Combustion and flame.* 2005; 140(4); 310-318.